Charging-free electrochemical system for harvesting low-grade thermal energy

Yuan Yang[a,1], Seok Woo Lee[b,1], Hadi Ghasemi[a,2], James Loomis[a], Xiaobo Li[a], Daniel Kraemer[a], Guangyuan Zheng[c], Yi Cui[b,d,3], and Gang Chen[a,3]

[a]Department of Mechanical Engineering, Massachusetts Institute of Technology, Cambridge, MA 02139; [b]Department of Materials Science and Engineering, Stanford University, Stanford, CA 94305; [c]Department of Chemical Engineering, Stanford University, Stanford, CA 94305; and [d]Stanford Institute for Materials and Energy Sciences, SLAC National Accelerator Laboratory, Menlo Park, CA 94025

Efficient and low-cost systems are needed to harvest the tremendous amount of energy stored in low-grade heat sources (<100 °C). Thermally regenerative electrochemical cycle (TREC) is an attractive approach which uses the temperature dependence of electrochemical cell voltage to construct a thermodynamic cycle for direct heat-to-electricity conversion. By varying temperature, an electrochemical cell is charged at a lower voltage than discharge, converting thermal energy to electricity. Most TREC systems still require external electricity for charging, which complicates system designs and limits their applications. Here, we demonstrate a charging-free TREC consisting of an inexpensive soluble $Fe(CN)_6^{3-/4-}$ redox pair and solid Prussian blue particles as active materials for the two electrodes. In this system, the spontaneous directions of the full-cell reaction are opposite at low and high temperatures. Therefore, the two electrochemical processes at both low and high temperatures in a cycle are discharge. Heat-to-electricity conversion efficiency of 2.0% can be reached for the TREC operating between 20 and 60 °C. This charging-free TREC system may have potential application for harvesting low-grade heat from the environment, especially in remote areas.

waste heat harvesting | Prussian blue analog | nanomaterials | batteries

A vast amount of low-grade heat (<100 °C) exists in industrial processes, environment, solar-thermal, and geothermal energy (1–3). It is generally difficult to convert such low-temperature thermal energy into electricity due to the distributed nature of heat sources and low-temperature differential. Different technologies, such as solid-state thermoelectric energy conversion (4–7) and organic Rankine cycles (1, 8), are being actively pursued but face their own challenges in efficiency, cost, and system complexity. Recently, a new thermally regenerative electrochemical cycle (TREC) based on a copper hexacyanoferrate (CuHCF) cathode and a Cu/Cu^{2+} anode was demonstrated by us for harvesting low-grade heat (9). A high efficiency of 5.7% was achieved when the cell was operated between 10 and 60 °C assuming a heat recuperation efficiency of 50% (9). TREC uses reversible electrochemical reactions to construct a thermodynamic cycle, and it is based on the temperature dependence of cell voltage (9–12). For a reversible full-cell reaction A+B → C+D (discharge), the temperature coefficient α is defined as

$$\alpha = \frac{\partial E}{\partial T} = -\frac{1}{nF}\frac{\partial \Delta G}{\partial T} = \frac{\Delta S}{nF}, \qquad [1]$$

where E is the full-cell voltage, T is the temperature, n is the number of electrons transferred in the reaction, and F is Faraday's constant. ΔG and ΔS are the partial molar Gibbs free energy and partial molar entropy change in full-cell reaction (12–14). To convert heat to electricity, the electrochemical cell is discharged from A+B to C+D at T_1 and recharged at a different temperature T_2 with lower voltage (Fig. 1 A and B). Consequently electricity is generated as the difference between the discharged and charged energy. The net electricity originates

from heat absorbed in electrochemical reactions at the higher temperature of T_1 and T_2 (10, 11). Such an electrochemical cycle is a thermodynamic Ericsson cycle with a theoretical efficiency of Carnot limit, as illustrated in the temperature-entropy diagram (*SI Appendix*, Fig. S1).

Our previous demonstration requires electricity to assist the regeneration (9); however, ideally a TREC system is regenerated only by thermal energy. This can be realized if the temperature change ($T_1 \rightarrow T_2$) shifts the electrode potential of the positive electrode to be lower than the negative electrode, or full-cell voltage to negative, indicating that ΔG for the reverse process at T_2 (C+D → A+B) is also negative (Fig. 1 C and D) and it corresponds to a spontaneous discharge instead of an electrically stimulated charge. Therefore, the system discharges at both T_1 and T_2, except that the polarity of the battery cell and the direction of spontaneous chemical reaction are opposite. This charging-free merit helps simplify system complexity and lower the cost, as no external electricity is needed. It is especially attractive for off-grid applications and self-powered devices (15, 16), where energy is simply provided by thermal fluctuation in environment. Only one example of such charging-free concept is found, however, the working temperature was over 300 °C and the system used toxic materials such as UF_6 and AsF_3 (17). Moreover, no experimental data were presented except the temperature dependence of open-circuit voltage (OCV). In this report, we experimentally demonstrate a charging-free aqueous electrochemical cell

Significance

Tremendous low-grade heat is stored in industrial processes and the environment. Efficient and low-cost utilization of the low-grade heat is critical to imminent energy and environmental challenges. Here, a rechargeable electrochemical cell (battery) is used to harvest such thermal energy because its voltage changes significantly with temperature. Moreover, by carefully tuning the composition of electrodes, the charging process is purely powered by thermal energy and no electricity is required to charge it. A high heat-to-electricity conversion efficiency of 2.0% can be reached when it is operated between 20 and 60 °C. Such charging-free characteristic may have potential application for harvesting low-grade heat from the environment, especially in remote areas.
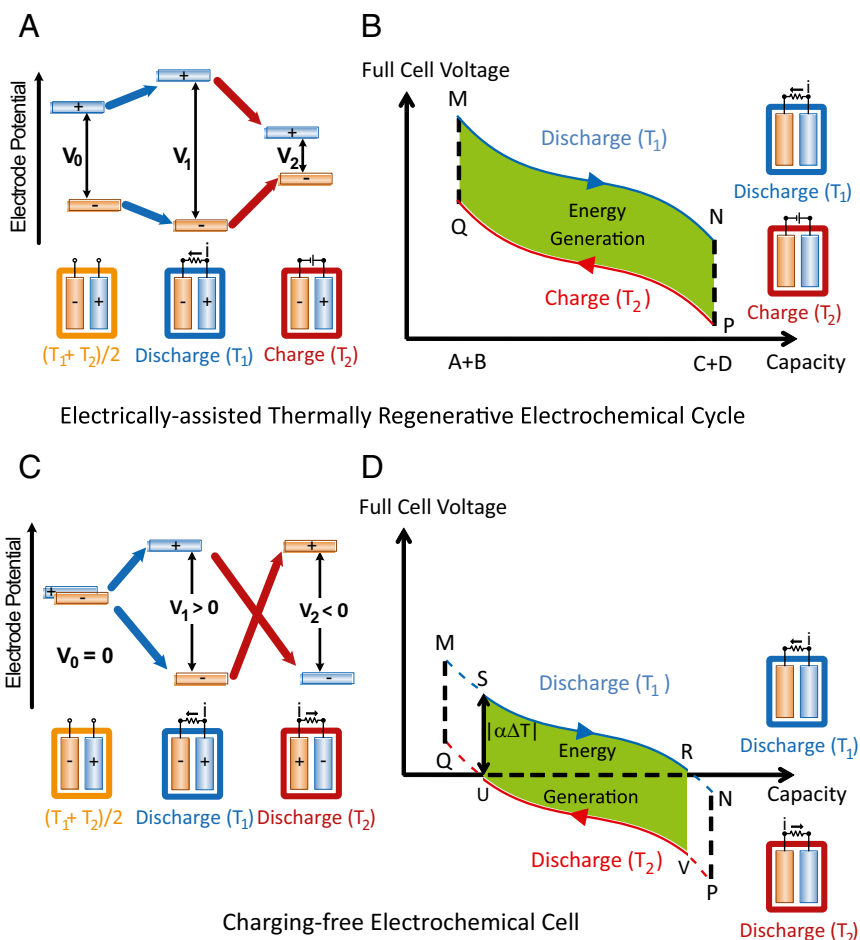
Fig. 1. Schematics of electrochemical cells to harvest thermal energy. (*A* and *B*) An electrically assisted TREC. (*A*) Changes in potential of both positive and negative electrodes in an electrically assisted thermal cycle. (*B*) The full-cell voltage–capacity plot in an electrically assisted thermal cycle. Net energy is generated as the discharge voltage is higher than charge voltage. However, external charging is needed in each cycle. (*C* and *D*) A charging-free TREC. (*C*) Changes in potential of both positive and negative electrodes in a charging-free thermal cycle. (*D*) The full-cell voltage–capacity plot in a charging-free thermal cycle. The voltage shift due to temperature change is large enough so that part of the full-cell voltage curve (UV) at T_2 is negative. This means if the operation is limited in the range of S→R→V→U, the polarity of the cell changes from T_1 to T_2, but the returning process (UV) is still spontaneous discharge ($\Delta G < 0$) instead of electrically stimulated charge, which regenerates the cell.

to harvest low-grade heat based on cheap and nontoxic materials. When cycled between 20 and 60 °C, its efficiency reaches 1.2% and 2.0% under a heat recuperation efficiency of 50% and 70%, respectively, which is attractive for low-grade heat harvesting.

Fig. 1 *C* and *D* illustrates several key points in searching for suitable electrochemical systems for charging-free cells. First, to realize polarity switch of the cell, the full-cell voltage should be approximately zero at $(T_1+T_2)/2$ for given T_1 and T_2 (Fig. 1*C*). The temperature at which the potentials of two electrodes are equal is defined as the cross-over temperature (T_{cross}). Second, a flat voltage curve is preferred. As shown in Fig. 1*D*, to avoid charging process (RN and UQ), only a part of voltage curve can be used (SR and UV). Because full-cell voltages at point R and U are both zero, the maximum voltage range that can be used is $|\alpha\Delta T|$ ($\Delta T = T_1 - T_2$) in a charging-free system. Consequently, to maximize charge capacity and thus energy output ($= |\alpha\Delta T| \times$ charge capacity), it is ideal to have a flat full-cell voltage curve.

Based on these criteria, 0.3 M $K_3Fe(CN)_6$/0.5 M $K_4Fe(CN)_6$ aqueous solution and Prussian blue $[KFe^{II}Fe^{III}(CN)_6, PB]$ are chosen as active materials for positive and negative electrodes, respectively, for a cycle demonstration between 20 and 60 °C, and the two electrodes are separated by Nafion ion-selective membrane (Fig. 2*A*). Here, the positive and negative electrodes are defined

as those at 20 °C. The electrolyte for PB is 2.5 M KNO_3 aqueous solution. At 20 °C, the potential of $Fe(CN)_6^{3-/4-}$ and half-discharged PB are 282 and 256 mV vs. Ag/AgCl/4M KCl reference electrode (Fig. 2*B*). Linear fitting shows that the temperature coefficients of $Fe(CN)_6^{3-/4-}$ and PB are -1.46 ± 0.02 and 0.00 ± 0.03 mV K^{-1}, respectively, between 20 and 65 °C, and the full-cell coefficient is -1.45 ± 0.03 mV K^{-1}. Therefore, T_{cross} is 37 °C as the potential of two electrodes are the same at 37 °C, and it is close to the midpoint of 20 and 60 °C. (Fig. 2*B*). A merit of $Fe(CN)_6^{3-/4-}$/PB system is that T_{cross} can vary to fit different temperature ranges (*SI Appendix*, Fig. S2). $Fe(CN)_6^{3-/4-}$ and PB are also well known for their high reversibility and low polarization (18, 19), which helps reduce the internal resistance and maximize the power capability. To further reduce the cell resistance, PB nanoparticles were synthesized by a simple solution approach with an average particle size of ~50 nm and drop cast onto carbon cloth current collector, as nanostructures increase surface area for reactions and reduce ionic diffusion length. (*SI Appendix*, Fig. S3). Carbon cloth was selected as the current collector for the soluble $Fe(CN)_6^{3-/4-}$ redox pair as it has high surface area. The full cell was tested in a home-made plastic cell with two electrodes separated by a piece of Nafion 115 membrane (*SI Appendix*, Fig. S4). Fig. 2*C* is a schematic of
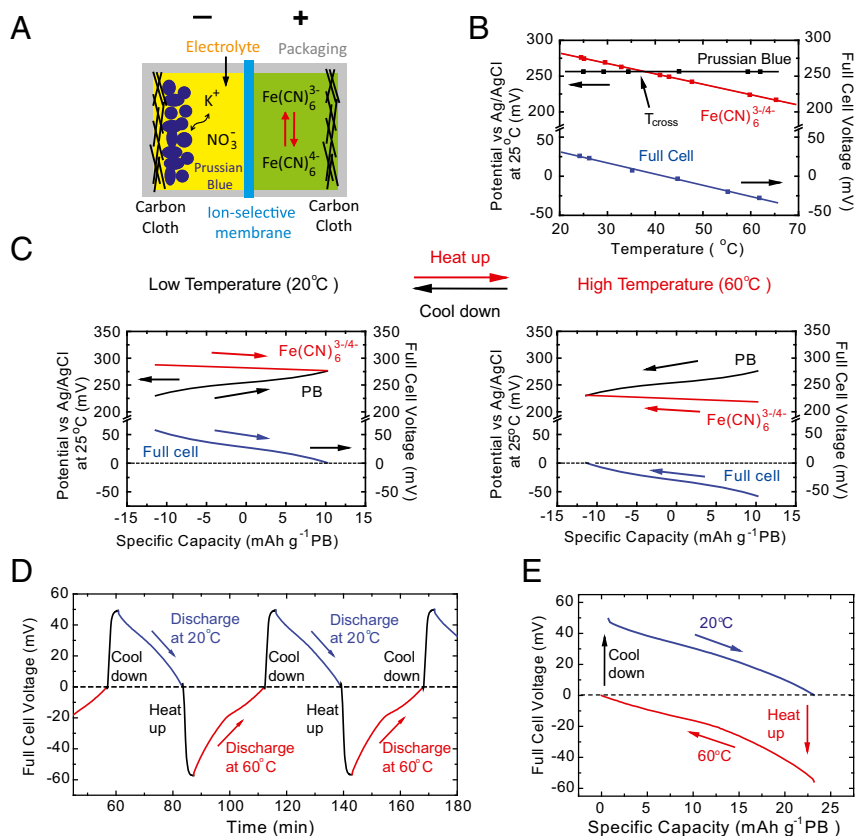
Fig. 2. Characteristics of the Fe(CN)$_6^{3-/4-}$/PB charging-free TREC system. (*A*) Schematic of the cell configuration. The two electrodes are separated by a piece of Nafion membrane. Positive and negative electrodes are defined as those at 20 °C. Details on cell assembly are shown in *SI Appendix*. (*B*) The dependence of electrode potential and full-cell voltage on temperature. The electrode potential is versus Ag/AgCl reference electrode with 4 M KCl at 25 °C. The temperature dependence of PB electrode and full-cell voltage was measured when PB was discharged to the midpoint of the voltage curve. The positive and negative electrodes switch with each other above the cross-over temperature (T$_{cross}$). (*C*) Voltage curves of electrodes and full cell at 20 and 60 °C. The arrows indicate the spontaneous reaction direction. As the absolute value of voltage goes down in both cases, they both correspond to discharge, but voltage polarity is reversed. (*D*) Cycling operation of the system in real time. At both 20 and 60 °C, the cell is discharged with a constant current of 60 mA g^{-1} to 0 mV. (*E*) The voltage vs. specific capacity plot of the cell in *D*. For *D* and *E*, the mass loading of PB is 5 mg and the volume of Fe(CN)$_6^{3-/4-}$ is 100 µL.

electrochemical processes of both electrodes and the full cell at 20 and 60 °C. At T$_L$ (20 °C), the cell is discharged from 55 mV to 0 mV (left to right) and electricity is produced. Then the cell is disconnected and heated. The electrode voltage of the Fe(CN)$_6^{3-/4-}$ redox pair shifts down due to its negative α while that of the PB electrode remains unchanged; thus the full-cell voltage shifts to −55 mV at T$_H$ (60 °C), indicating that the positive and negative electrodes are switched. The process at 60 °C is from right to left and the absolute value of the full-cell voltage decreases from 55 mV to 0 mV. Hence, it is discharge instead of charge but current is in the opposite direction to that at T$_L$. The last process is cooling the cell down to T$_L$ to complete the cycle.

Experimental results of a full cell cycled between 20 and 60 °C are shown in Fig. 2*D*. First, the cell was discharged to 0 mV at 20 °C starting from an OCV of 49 mV. Then the cell was heated to 60 °C by thermoelectric (TE) plates. During heating, OCV became negative and finally saturated at −57 mV, which means that the cell is still capable of discharge except that the polarity switches. After the cell was discharged to 0 mV again, it was cooled down to 20 °C by TE plates (*SI Appendix*, Fig. S4*F*). The difference between OCVs at 20 and 60 °C arises from the weak dependence of α on state of charge (*SI Appendix*, Fig. S6), which leads to slightly different magnitudes of voltage change in cooling and heating. The whole cycle is also plotted as voltage versus specific capacity (Fig. 2*E*). It is clear that the voltage curves at both 20 and 60 °C have the same shape, and the temperature

effect shifts the curve down without affecting the nature of the electrochemical reactions. The specific capacity discharged is 23 mAh g^{-1} based on the mass of PB, which is less than half of its common capacity (60 mAh g^{-1}). This is because the potential difference between two electrodes must be less than the voltage change due to the temperature effect ($|\alpha\Delta T|$), as discussed before.

Fig. 3 *A* and *B* illustrates the cycling performance of this charging-free system for T$_H$/T$_L$ of 60/20 °C. The cell is cycled under N$_2$ as oxygen has an adverse effect on the cycling of PB, as O$_2$ can oxidize PB in the discharged state whereas O$_2$ is reduced to water (20, 21). (Fig. 3*C* and *SI Appendix*, Fig. S7). The current rate is 60 mA g^{-1}. For capacity, good cycling was observed for discharges at both 60 and 20 °C (Fig. 3*A*). Capacity fading due to drying out of electrolyte was observed after 10 cycles, as the cell was not fully sealed for the purpose of pressure balance. However, after adding more water (indicated by the asterisk), the specific capacity was fully recovered. Similar behavior was observed in the plot of specific energy against cycle number (Fig. 3*B*). The discharged energy at 20 °C shows a steady cycling, whereas that at 60 °C had a notable drop after 10 cycles but fully recovered after adding water. To further prove that the fading is due to solvent evaporation, cells with excessive amount of electrolyte are tested and both Fe(CN)$_6^{3-/4-}$ and PB electrodes show stable cycling over 500–1,000 cycles (Fig. 3 *C* and *D* and *SI Appendix*, Fig. S7; see more information in *SI Appendix*). In addition, although charge capacities at 20 and 60 °C are very
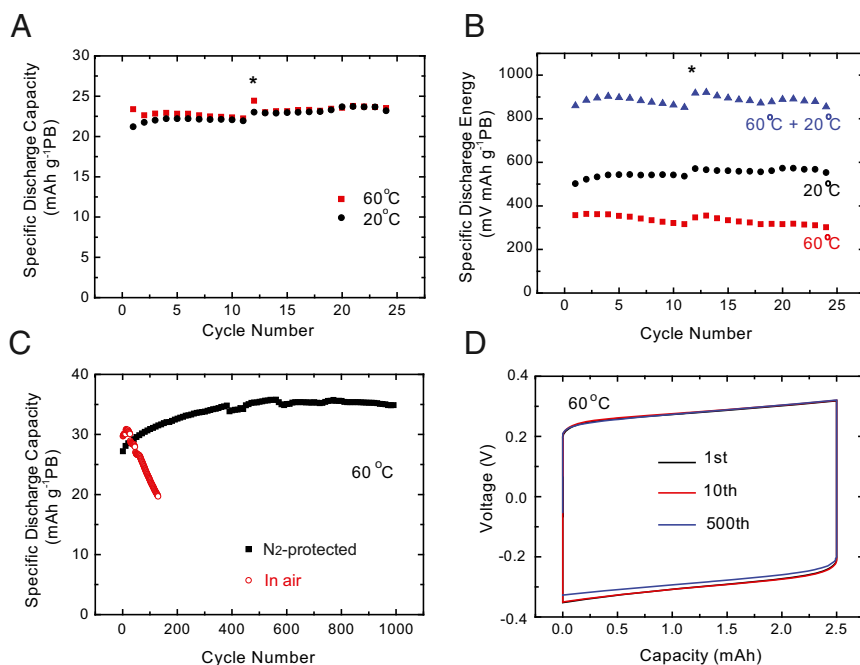
Fig. 3. Cycling performance of $Fe(CN)_6^{3-/4-}$/PB charging-free system. (*A* and *B*) Thermal cycling of $Fe(CN)_6^{3-/4-}$/Prussian cell. The temperature switches between 20 and 60 °C. (*A*) The specific discharge capacity and (*B*) the specific discharge energy of the system based on the mass of PB. The volume of $Fe(CN)_6^{3-/4-}$ and the mass of PB are ~100 μL and 5–6 mg, respectively. Discharges at both temperatures were done with a current rate of 60 mA g^{-1} to 0 mV. The asterisk (*) indicates adding more water to compensate evaporation loss. (*C* and *D*) Cycling performance of (*C*) PB and (*D*) $Fe(CN)_6^{3-/4-}$ at 60 °C. The test at 60 °C is to evaluate the stability of these materials at high temperature. As only ~25 mAh g^{-1} capacity of PB was used in full-cell cycling, the PB electrode was cycled with a specific capacity of ~30 mAh g^{-1}. The currents for PB and $Fe(CN)_6^{3-/4-}$ are 600 mA g^{-1} and 6 mA cm^{-2}, respectively. Test on $Fe(CN)_6^{3-/4-}$ is done in air. More details on cycling test at 60 °C are discussed in *SI Appendix*.

close, the specific energy at 20 °C is obviously higher than that at 60 °C. This is because the voltage profile at 20 °C is concave and thus the average voltage at 20 °C is higher. For long-term operation, diffusion of $Fe(CN)_6^{3-/4-}$ through Nafion membrane could be an issue which requires further investigation. Engineering membrane to be more selective to anions may help solve this problem.

TREC has a theoretical efficiency of Carnot limit. In practical operation, effects of the heat capacity and the internal resistance need to be taken into account, limiting the efficiency to a fraction of Carnot. We calculated the heat-to-electricity conversion efficiency (η) for the cycle above and it is based on the procedure discussed in our previous publication (9).

$$\eta = \frac{W}{Q_H + Q_{HR}} = \frac{W_{20°C} + W_{60°C}}{\alpha T_H Q_c + (1 - \eta_{HR})C_p \Delta T},$$ [2]

where W is the total amount of energy discharged at both T_H and T_L in a cycle. Q_H is the heat absorbed at T_H (60 °C). Q_{HR} is the extra energy needed to heat the cell up. Q_c is the discharge capacity at T_H, C_p is the heat capacity of the cell. η_{HR} is the heat recuperation efficiency, indicating how much energy rejected in the cooling process can be used for the heating process, and 50–70% is reasonable as demonstrated in our previous work (9). η is a function of the ratio (ϕ) of $Fe(CN)_6^{3-/4-}$ volume to PB mass, as total heat capacity depends on ϕ (Fig. 4*A*). The blue dots were calculated based on experimental discharge energy of a real cell. For further optimization, voltage curves at different ϕ were simulated at two conditions: (*i*) no overpotential (dashed lines in Fig. 4*A*), which represents the efficiency limit of the system, and (*ii*) overpotential of 10 mV (solid lines), which is close to the overpotential in real operations. Heat recuperation efficiency (η_{HR}) of 50% (red) and 70% (black) were considered. At η_{HR} of 70% and no overpotential (dashed black line), the cell can

reach a maximum efficiency of 2.0% at $\phi \sim 1$ mL g^{-1} (*SI Appendix*, Figs. S8 and S9). As our experimental results show that the overall overpotential at 20 and 60 °C was 10 mV (*SI Appendix*, Fig. S10), the heat-to-electricity efficiency with 10-mV overpotential considered was simulated too (solid lines). The simulation matches well with experimental results, and η reaches 1.5% at optimal ratio of $Fe(CN)_6^{3-/4-}$ volume to PB mass ($\eta_{HR} = 70\%$). The volcano shape of efficiency versus ϕ (Fig. 4*A*) arises from the competition between heat capacity and charge capacity. When the amount of $Fe(CN)_6^{3-/4-}$ catholyte increases, its contribution to the change of full-cell voltage becomes smaller; thus the charge capacity and electricity produced in a cycle are larger (*SI Appendix*, Fig. S9). However, this happens at the cost of a higher heat capacity requiring larger energy input in the heating process. These two factors compete with each other and the optimal ϕ is ~1 mL g^{-1}. The heat-to-electricity efficiency of this charging-free system is lower than our previous report (9) on the (CuHCF)//Cu^{2+}/Cu system. There are two reasons: (*i*) $Fe(CN)_6^{3-/4-}$ has a low solubility in water which limits the charge capacity, and (*ii*) only ~1/3 of PB's theoretical capacity is used to prevent electrical charging. However, this efficiency is still much higher than thermogalvanic cells, another strategy based on the temperature effect of electrochemical reactions but with the same architecture as TE devices (13, 22).

The overall heat-to-electricity efficiency (η) also depends on η_{HR} (Fig. 4*B*). When no heat recuperation is used ($\eta_{HR} = 0$), which simplifies the design, efficiency is 0.68% and 0.52% for 0- and 10-mV overpotential, respectively, and it is about threefold that of thermogalvanic cells (22, 23). Moreover, we have shown before that heat recuperation efficiency (η_{HR}) in 50–70% can be readily achieved, and even higher efficiency is possible (9). The corresponding heat-to-electricity conversion efficiencies are shown above. As TE devices are major candidates for waste heat harvesting, there are noticeable differences between these two
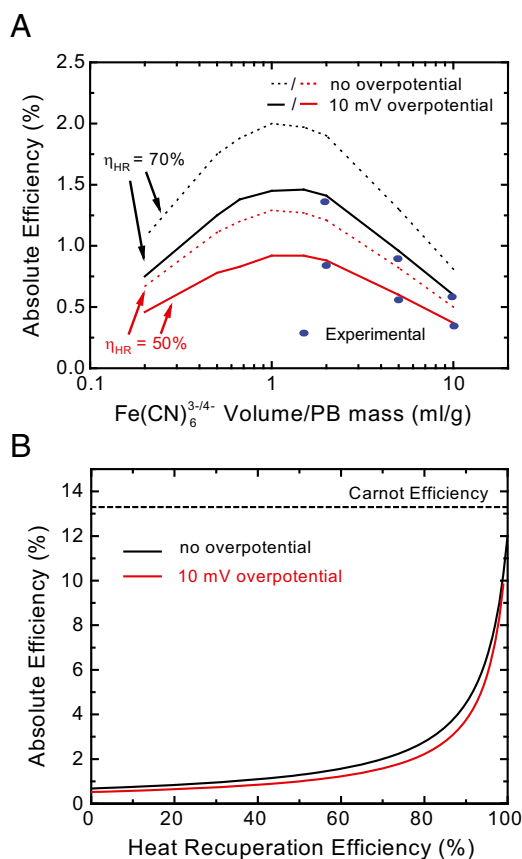
Fig. 4. Absolute heat-to-electricity conversion efficiency (η) of the Fe(CN)$_6^{3-/4-}$/PB charging-free system. (*A*) The dependence of absolute efficiency on the ratio of the Fe(CN)$_6^{3-/4-}$ catholyte volume to the mass of PB. The blue dots are experimental data whereas the black and red curves are simulation results based on experimental voltage curves. Heat recuperation efficiency (η_{HR}) of 50% and 70% are shown. (*B*) The dependence of absolute conversion efficiency on the heat recuperation efficiency.

approaches. Temperature gradient is required for TE operation. In contrast, TREC works under isothermal process, which is easier for thermal management at low temperature. However, although TRECs may have higher efficiency, their power density is on the order of 1 mW g^{-1} based on the weight of active materials in both electrodes and electrolytes, lower than TE devices. Further analysis on effects of other factors, such as packaging and system level management, is needed to understand cost and power generation at the system level.

In addition, there are challenges in long-term operation for TREC (9). With these differences borne in mind, it is interesting to compare efficiencies above with TE devices working between the same T_H and T_L. For T_H/T_L of 60/20 °C, efficiencies of 2.0% and 1.5% ($\eta_{HR} = 70\%$) would require an ideal TE device with average figure of merit ZT of 0.90 and 0.65, respectively. Current TE materials have ZT of 1–1.5 for temperature below 100 °C (7, 24). If further optimization can realize η_{HR} of 85%, η will reach 3.2% and 2.3% for 0- and 10-mV overpotential, respectively, leading to equivalent ZT of 2.1 and 1.5. Further improvement in power density and efficiency can be realized through reducing internal resistance of electrodes, searching for new materials with high positive temperature coefficients and figures of merit for TREC (Y) (9).

In summary, a charging-free electrochemical system is demonstrated for harvesting low-grade heat. The cell consists of Fe(CN)$_6^{3-/4-}$ redox pair as active material for positive electrode and a solid PB nanoparticle negative electrode. When temperature changes from 20 to 60 °C, the cell voltage becomes negative, indicating that the cell polarity switches but it is still capable of discharging. This charging-free character originates from the fact that temperature changes the magnitude of TΔS and thus ΔG of the full-cell reaction are negative for both T_L and T_H. The system exhibits reasonable cycling performance. Its heat-to-electricity conversion efficiency reaches 2% with heat recuperation considered, equivalent to ZT of 0.9 for TE devices working between the same hot and cold sources. The efficiency is about one order of magnitude higher than previous studies on thermogalvanic cells (22). This system is attractive for harvesting low-grade heat because it uses inexpensive materials and the charging-free characteristic could simplify the system design. It may have potential application for harvesting thermal energy from the environment, such as temperature alternation of day and night, especially in remote areas.

Methods

Material Preparation. All chemicals were purchased from Sigma-Aldrich. To synthesize PB, 40 mL of 50 mM FeCl$_2$ was dropped in 40 mL of 25 mM K$_3$Fe(CN)$_6$ under strong stirring at room temperature. The precipitation was centrifuged and dried at 70 °C overnight (25, 26). The PB electrode was prepared by mixing 70 wt % PB nanoparticles, 20 wt % Super P carbon black, and 10% polyvinylidene fluoride in *N*-methyl-2-pyrrolidone and drop cast onto carbon cloth disk electrode (Fuel Cell Store) at 90 °C. The carbon cloth disk had a diameter of 1.27 cm and the mass loading is about 5 mg PB cm^{-2}. The electrolyte for the PB electrode is 2.5 M KNO$_3$ aqueous solution. 0.5 M K$_4$Fe(CN)$_6$/0.3 M K$_3$Fe(CN)$_6$ catholyte was prepared by dissolving corresponding chemicals in deionized water. A carbon cloth electrode disk with diameter of 1.27 cm served as current collector for the catholyte. Nafion 115 membrane was used to separate the liquid catholyte from the anode. The membrane was pretreated with concentrated sulfuric acid for 2 h and stored in 0.5 M KNO$_3$ aqueous solution before use.

Cell Assembly and Electrochemical Measurement. Measurements on the temperature coefficient of electrodes were performed against a calibrated Ag/AgCl/4 M KCl reference electrode (Fisher Scientific) in a three-neck flask. The temperature coefficient of the reference electrode is measured to be 0.12 ± 0.02 mV/K. A home-made plastic cell is used for all full-cell measurements (*SI Appendix*, Fig. S4). The PB electrode with current collector is first attached to 25-μm-thick Pt foil. Then they were inserted into the home-made plastic cell. The two electrodes were separated by a Nafion 115 membrane. The top of Nafion film is intentionally left higher than the top of electrolytes to avoid intermixing. Then the Fe(CN)$_6^{3-/4-}$ catholyte and the KNO$_3$ electrolyte were injected into each side through holes on top of the plastic cell. Temperature cycling of full cells was performed in a home-made TE plate-based thermal cycler in a N$_2$ box. More details on cell assembly can be found in *SI Appendix*. For high-temperature cycling of PB electrode, a beaker cell was constructed with excessive Fe(CN)$_6^{3-/4-}$ as the counter-electrode (*SI Appendix*, Fig. S5). High-temperature cycling of Fe(CN)$_6^{3-/4-}$ catholyte was done in a symmetric configuration by injecting the solution to both sides of the plastic cell. All electrochemical measurements were done with a Bio-Logic VSP300 tester.

1. Chu S, Majumdar A (2012) Opportunities and challenges for a sustainable energy future. *Nature* 488(7411):294–303.

2. Gur I, Sawyer K, Prasher R (2012) Engineering. Searching for a better thermal battery. *Science* 335(6075):1454–1455.

3. Rattner AS, Garimella S (2011) Energy harvesting, reuse and upgrade to reduce primary energy usage in the USA. *Energy* 36(10):6172–6183.

4. Zebarjadi M, Esfarjani K, Dresselhaus MS, Ren ZF, Chen G (2012) Perspectives on thermoelectrics: From fundamentals to device applications. *Energy & Environmental Science* 5(1):5147–5162.

5. Biswas K, et al. (2012) High-performance bulk thermoelectrics with all-scale hierarchical architectures. *Nature* 489(7416):414–418.

6. Snyder GJ, Toberer ES (2008) Complex thermoelectric materials. *Nat Mater* 7(2): 105–114.

7. Poudel B, et al. (2008) High-thermoelectric performance of nanostructured bismuth antimony telluride bulk alloys. *Science* 320(5876):634–638.

8. Tchanche BF, Lambrinos G, Frangoudakis A, Papadakis G (2011) Low-grade heat conversion into power using organic Rankine cycles - A review of various applications. *Renew Sustain Energy Rev* 15(8):3963–3979.

9. Lee SW, et al. (2014) An electrochemical system for efficiently harvesting low-grade heat energy. *Nat Commun* 5:3942.

10. Chum HL, Osteryoung RA (1980) Review of thermally regenerative electrochemical systems. *Synopsis and Executive Summary* (Solar Energy Research Institute, Golden, CO), Vol 1.

11. Anderson LB, Greenberg SA, Adams GB (1967) Thermally and photochemically regenerative electrochemical systems. *Adv Chem Ser* 64:213–276.

12. Debethune AJ, Licht TS, Swendeman N (1959) The temperature coefficients of electrode potentials - the isothermal and thermal coefficients - the standard ionic entropy of electrochemical transport of the hydrogen ion. *J Electrochem Soc* 106(7):616–625.

13. Quickenden TI, Mua Y (1995) A review of power-generation in aqueous thermogalvanic cells. *J Electrochem Soc* 142(11):3985–3994.

14. Kuzminskii YV, Zasukha VA, Kuzminskaya GY (1994) Thermoelectric effects in electrochemical systems - nonconventional thermogalvanic cells. *J Power Sources* 52(2): 231–242.

15. Wang ZL, Wu W (2012) Nanotechnology-enabled energy harvesting for self-powered micro-/nanosystems. *Angew Chem Int Ed Engl* 51(47):11700–11721.

16. Xu S, et al. (2010) Self-powered nanowire devices. *Nat Nanotechnol* 5(5):366–373.

17. McCully CR (1967) US Patent 3,318,734.

18. Pharr C, Griffiths P (1997) Infrared spectroelectrochemical analysis of adsorbed hexacyanoferrate species formed during potential cycling in the ferrocyanide/ferricyanide redox couple. *Anal Chem* 69(22):4673–4679.

19. Stilwell DE, Park KH, Miles MH (1992) Electrochemical studies of the factors influencing the cycle stability of Prussian Blue films. *J Appl Electrochem* 22(4):325–331.

20. Itaya K, Shoji N, Uchida I (1984) Catalysis of the reduction of molecular-oxygen to water at Prussian blue modified electrodes. *J Am Chem Soc* 106(12):3423–3429.

21. Agrisuelas J, et al. (2007) Usefulness of F(dm/dQ) function for elucidating the ions role in PB films. *J Electrochem Soc* 154(6):F134–F140.

22. Hu R, et al. (2010) Harvesting waste thermal energy using a carbon-nanotube-based thermo-electrochemical cell. *Nano Lett* 10(3):838–846.

23. Gunawan A, et al. (2013) Liquid thermoelectrics: Review of recent and limited new data of thermogalvanic cell experiments. *Nanoscale Microscale Thermophys Eng* 17(4):304–323.

24. Liu W-S, et al. (2011) Thermoelectric property studies on Cu-doped n-type $Cu_xBi_2Te_{2.7}Se_{0.3}$ nanocomposites. *Adv Energy Mater* 1(4):577–587.

25. Lu Y, Wang L, Cheng J, Goodenough JB (2012) Prussian blue: A new framework of electrode materials for sodium batteries. *Chem Commun (Camb)* 48(52):6544–6546.

26. Wessells CD, Huggins RA, Cui Y (2011) Copper hexacyanoferrate battery electrodes with long cycle life and high power. *Nat Commun* 2:550.